

## *Chandra* Observations of the Luminous, O-Rich SNR in the Irregular Galaxy NGC 4449

Daniel J. Patnaude & Robert A. Fesen

*6127 Wilder Laboratory, Physics & Astronomy Department  
Dartmouth College, Hanover, NH 03755*

### ABSTRACT

An analysis of a 29 ksec *Chandra* ACIS-S observations of the young, Cassiopeia A-like supernova remnant in the irregular galaxy NGC 4449 is presented. The observed 0.5 – 2.1 keV spectrum reveals the likely presence of several emission lines including O VIII at 0.65 and 0.77 keV, Ne X at 1.05 keV, Mg XI at 1.5 keV, and Si XIII at 1.85 keV. From the observed spectrum, we derive an  $N_{\text{H}} = 1 \times 10^{21} \text{ cm}^{-2}$  and an X-ray temperature of  $T \approx 9 \times 10^6 \text{ K}$ . A non-equilibrium ionization fit to the spectrum suggests an overabundance of oxygen around 20 times solar, consistent with the remnant's UV and optical emission-line properties. We discuss the remnant's approximate X-ray derived elemental abundances and compare its X-ray spectrum and luminosity to other oxygen-rich remnants.

*Subject headings:* galaxies: individual – nebulae: supernova remnants – X-rays: sources

### 1. INTRODUCTION

At present, there are only about a half-dozen O-rich supernova remnants (SNRs) known. They represent the remains of high-mass stars ( $M \gtrsim 15 M_{\odot}$ ) and thus are especially useful for studying the elemental abundances of explosive nucleosynthesis processes in core-collapse supernovae. The younger the remnant is, the more likely its properties accurately reflect true SN ejecta abundances unaffected by dilution from swept-up circumstellar and interstellar material.

Currently, the youngest Galactic remnant is the  $\simeq 320$  yr old O-rich SNR Cassiopeia A (Cas A). However, with an estimated age of around 100 yr (Blair, Kirshner, & Winkler 1983;

Blair & Fesen 1998), the O-rich SNR located in the Magellanic type irregular galaxy NGC 4449 represents the youngest example of this type of remnant and is therefore an object of particular interest.

The NGC 4449 SNR was first identified by Seaquist & Bignell (1978), who found a strong and point-like, non-thermal radio source approximately  $1'$  north of the nucleus of this galaxy coincident with an H II region cataloged by Sabbadin & Bianchini (1979). Optical spectrophotometry of this source by Balick & Heckman (1978) showed two components: (1) narrow lines belonging to a conventional H II region, and (2) broad [O III]  $\lambda\lambda 4959, 5007$  and [O I]  $\lambda\lambda 6300, 6363$  line emissions which they attributed to a young SNR similar to Cas A.

Optical and UV spectra taken by Kirshner & Blair (1980), Blair, Kirshner, & Winkler (1983), and Blair et al. (1984) confirmed and extended this interpretation and yielded a rough analysis of the physical conditions in the SNR and the associated H II region. They found optical line widths implying an expansion velocity of  $3500 \text{ km s}^{-1}$  and emphasized the extremely low abundance of hydrogen in the ejecta. Furthermore, they estimated that the total mass of oxygen in the optical was  $10^{-2} M_{\odot}$ , some 50 times higher than the value derived for Cas A (Peimbert 1971), and estimate a progenitor mass  $\approx 30 M_{\odot}$ .

Using data from the *Einstein X-Ray Observatory* High Resolution Imager, Blair, Kirshner, & Winkler (1983) found the SNR to also be highly luminous in X-rays, with  $L_x \approx 10^{39} \text{ erg s}^{-1}$  assuming a distance of 5.0 Mpc. Even at a smaller estimated distance of 3.9 Mpc (de Vaucouleurs et al. 1991; Hunter, van Woerden, & Gallagher 1999), this SNR is nearly 10 times more luminous in X-rays than Cas A, the most luminous young SNR in our Galaxy, and several times more luminous than the bright O-rich SNR N132D in the Large Magellanic Cloud ( $L_x \approx 6 \times 10^{37} \text{ erg s}^{-1}$ ; Hughes 1987).

More recently, Vogler & Pietsch (1997) studied *ROSAT* PSPC and HRI detected NGC 4449 sources, including the SNR. They were able to fit the remnant's spectrum to an absorbed thermal bremsstrahlung model, reporting a lower limit on both the absorbing column  $N_H \geq 7 \times 10^{20} \text{ cm}^{-2}$  and temperature of  $\geq 600 \text{ eV}$  corresponding to  $T \geq 7 \times 10^6 \text{ K}$ . They also found a  $L_x$  of  $\approx 1.8 \times 10^{38} \text{ erg s}^{-1}$ , a value about 50% that of the Blair et al. (1983) *Einstein* 1978 estimate.

Here we report on observations of the SNR in NGC 4449 obtained with the *Chandra X-ray Observatory* (Weisskopf, O'Dell, & van Speybroeck 1996). In §2 we describe the observations and data reduction. In §3 we discuss our model fits to the data, the derivation of various physical quantities associated with the X-ray emitting plasma, and how the SNR compares to other O-rich SNR. Our results and conclusions are summarized in §4.

## 2. Observations and Data Reduction

We have analysed an archival 29 ksec exposure of NGC 4449 obtained on 4 Feb 2001 (ObsID No.2031; PI: T. Heckman) with the S3 chip of the Advanced CCD Imaging Spectrometer (ACIS; Garmire et al. 1992; Bautz et al. 1998). ACIS-S3 is a back-side-illuminated CCD with low to moderate spectral resolution ( $E/\Delta E \sim 4.3$  at 0.5 keV;  $E/\Delta E \sim 30$  at 5.9 keV). We used *Chandra X-Ray Observatory* center level 1 and level 2 event lists, and the *ASCA*-like [0, 2, 3, 4, 6] grade set.

The *Chandra* ACIS image of the SNR is shown in Figure 1. For comparison, we also show the Einstein HRI and ROSAT HRI images. In previous observations, it is clear that there is source confusion with two X-ray sources located  $\approx 10''$  to the southwest. However, the *Chandra* observation does not suffer from this source confusion, and we can separate the SNR from surrounding sources. We note that the position of the SNR is coincident with the radio source as identified by Seaquist & Bignell (1978).

The data were calibrated and background subtracted using the *Chandra Interactive Analysis of Observations* (CIAO) software (Version 2.2) along with the Version 2.15 of the calibration database. A spectrum was extracted from a circle of 10 pixel radius ( $\approx 5''$ ) centered on the source. While Blair & Fesen (1998) quote an upper limit of 0.6 pc ( $0'.028$ ) on the size of the remnant, the point spread function of the telescope produces only 76% of the encircled energy within a  $1''$  diameter aperture (Jerius et al. 2000). Given that the SNR is isolated with respect to other sources in NGC 4449, we chose an aperture of  $\approx 10''$ , where 99% of the source emission is detected. A background spectrum located  $\approx 15''$  to the northeast of the SNR was also extracted.

To help identify potential line features in the low S/N spectrum, we compared the NGC 4449 SNR spectrum to those of other O-rich SNRs. Using the archival *Chandra* observation (ObsID No. 126) of G292.0+1.8, we extracted the spectrum of the entire remnant. Because of variations in the ACIS-S quantum efficiency, the  $12' \times 8'$  remnant was binned into  $0'.74 \times 0'.74$  ( $90 \times 90$  pixels) bins. The spectrum from each bin was extracted, and we summed all the individual spectra. The summed spectrum was then convolved with an energy and position weighted response matrix, as calculated by the CIAO task “*mkwarf*”. A similar procedure was followed to extract summed spectra for *Chandra* observations of Cas A (ObsID No. 114) and 1E 0102-7219 (ObsID No. 1231).

### 3. Results and Discussion

The *Chandra* ACIS spectrum of the NGC 4449 SNR for 0.5 to 2.1 keV is shown in Figure 2. Using PI binning, the data were binned by a factor of four, reducing the total number of pulse height channels from 4096 to 1024. The observed background subtracted count rate was  $(3.8 \pm 0.2) \times 10^{-2}$  counts s<sup>-1</sup>. Although the full spectral range of ACIS is 0.1 to 9.0 keV, we have limited our analysis of the NGC 4449 SNR X-ray spectrum to between 0.5 to 2.1 keV. Inspection of the data showed few detected events above 2.1 keV and below 500 eV.

Despite the low counts per channel ( $< 25$ ), five likely emission features can be seen in the extracted spectrum (see Fig. 2). The clearest ones are what appear to be Ne X at 1.05 keV and emission around the Si-K complex of lines near 1.85 keV. We also note the possible detection of O VIII at 654 and 774 eV, and Mg XI at 1.5 keV.

For comparison, we also show in Figure 2 our *Chandra* ACIS summed spectrum of the Galactic O-rich SNR G292.0+1.8. One can see that there is a general resemblance of the NGC 4449 SNR spectrum to that of G292.0+1.8 in that several emission features seem to be present in both and with similar strength (e.g., for example, O VIII, Mg XI, and Si XIII emission features.) Because of this resemblance, we have used the *Chandra* G292.0+1.8 spectrum as a template to identify possible weak features in NGC 4449 SNR. Specifically, G292.0+1.8 shows the presence of very weak Ne IX and Mg XII emissions. In spite of the relatively low quality of the NGC 4449 SNR spectrum, there are some indications for the presence of both lines, but with different relative strengths compared to SNR G292.0+1.8. That is, the NGC 4449 SNR spectrum hints at weaker Ne IX emission relative to Ne X than that seen in G292.0+1.8.

#### 3.1. Spectral Fitting

Because of the spectral similarity of the NGC 4449 SNR with G292.0+1.8, we have employed the results of an *Einstein* analysis of G292.0+1.8 (Hughes & Singh 1994) as a starting point for estimating the X-ray emission temperature and elemental abundances for the NGC 4449 SNR.

The ACIS spectrum of the NGC 4449 SNR was fit to a non-equilibrium ionization (NEI) model with variable abundances, corrected for Galactic absorption. Due to the low quality of the data, the spectral fits were overparametrized ( $\chi^2_{red} \sim 0.6$ ). However, a weighting scheme developed by Churazov et al. (1996), whereby the weight for a given data channel is estimated by averaging the counts in surrounding channels, significantly improved the quality of the

model fits ( $\chi_{red}^2 \sim 1.1$ ). The resulting best fit is shown in Figure 3. Table 1 lists our best fit values for the plasma temperature (kT), absorbing column density ( $N_H$ ), and ionization timescale ( $n_e t$ ). The quoted errors are at 90% confidence for the 10 free parameters. For comparison, we also list the results of Hughes & Singh (1994) for G292.0+1.8. Our best fit values of  $N_H = 1.7 \times 10^{21} \text{ cm}^{-2}$  and  $T \approx 9.2 \times 10^6 \text{ K}$ , corresponding to a shock velocity of  $830 \text{ km s}^{-1}$ . These compare favorably with the Vogler & Pietsch (1997) values of  $N_H \geq 0.7 \times 10^{21}$  and  $T \geq 7 \times 10^6 \text{ K}$ . Our value for  $N_H$  also agrees well with the value derived by Blair, Kirshner, & Winkler (1983),  $N_H = 1.5 \times 10^{21} \text{ cm}^{-2}$  which was based on optical measurements.

Our resulting modeled 0.5–2.1 keV X-ray flux for the NGC 4449 remnant is  $(8.6 \pm 1.3) \times 10^{-14} \text{ erg cm}^{-2} \text{ s}^{-1}$ , which at a distance of 3.9 Mpc, corresponds to  $L_x = 2.4 \times 10^{38} \text{ erg s}^{-1}$ . This is in reasonably good agreement with the value quoted by Vogler & Pietsch (1997) of  $L_x \approx 1.8 \times 10^{38} \text{ erg s}^{-1}$ . However, it is about half the  $5 \times 10^{38} \text{ erg s}^{-1}$  value (at a revised distance of 3.9 Mpc) determined from *Einstein* HRI measurements by Blair, Kirshner, & Winkler (1983). While the cause for this discrepancy may be due to a real decrease in X-ray flux (see Section 3.3 below), the *Einstein* HRI measurement was based on data covering a wider energy band (0.2–4 keV) and was modeled with a Raymond-Smith plasma assuming solar abundances.

Although the ACIS spectrum of the NGC 4449 SNR is of low S/N, it is still possible to estimate some physical parameters of the remnant’s X-ray emitting plasma. We first estimated the mass of ejecta which is currently emitting in X-rays. We began by assuming a simple geometry for the remnant’s X-ray emission structure and then use a spectral model, such as our NEI model, to relate the observed X-ray emissivity to the volume emission measure. Given that the source is unresolved, we assumed a spherical geometry. Then, adopting a remnant radius of 0.3 pc (Blair & Fesen 1998), the total volume of the emitting region is  $V = 3.1 \times 10^{54} f D_{3.9\text{Mpc}}^3 \text{ cm}^3$ , where  $D_{3.9\text{Mpc}}$  is the distance to the remnant, normalized to 3.9 Mpc and  $f$  is the volume filling factor. The root mean square hydrogen number density is determined from the model normalization, which is just the volume emission measure,  $n_e n_H V$ , for a known distance and geometry.

From Table 1,  $n_e n_H V = (5.5 \pm 0.05) \times 10^{60} \text{ cm}^{-3}$ . Using  $n_e/n_H = 1.47$ , consistent with the ratio used by Hughes & Singh (1994), and the expression for the emitting volume above, the root mean square hydrogen number density is  $n_H = 1.1 \times 10^3 f^{-0.5} D_{3.9\text{Mpc}}^{-0.5} \text{ cm}^{-3}$ . Using this expression, we estimate the mass of the X-ray emitting gas, including the mass of metals as well as He and H, to be  $M = 5.7 f^{0.5} D_{3.9\text{Mpc}}^{2.5} M_\odot$ .

We have also used the *Chandra* spectrum to estimate elemental abundances within the remnant ejecta. In Table 1, we list the volumetric emission measure for each element we

fit, scaled to solar values. By again assuming an  $n_e/n_H$  of 1.47, we determined the relative abundances for each element listed. For a particular element, the abundance relative to solar is given by:

$$\frac{(X/H)}{(X/H)_\odot} = n_e n_H V \frac{n_X/n_H}{(X/H)_\odot} .$$

Consequently, our estimated abundances for O, Ne, Mg, Si, and Fe are 18, 15, 9.0, 9.0, and 2.2 by number, respectively. The high overabundance of oxygen is consistent with the remnant’s UV and optical spectrum which is dominated by strong oxygen line emissions (Kirshner & Blair 1980; Blair et al. 1984).

### 3.2. Comparisons to Other Oxygen-Rich SNRs

X-ray and optical properties for five of the seven currently known O-rich SNRs are listed in Table 2. For each remnant other than the one in NGC 4449, unabsorbed fluxes and luminosities are listed for the energy range 0.3 – 2.1 keV. These values were obtained by fitting a two component thermal plasma with variable abundances to the total SNR spectra (Seward et al. 2002).

With an X-ray luminosity of  $2.4 \times 10^{38}$  erg s<sup>-1</sup>, the NGC 4449 SNR is clearly the most luminous O-rich SNR relative to the the four other O-rich SNRs listed in Table 2, which includes Cas A. The origin of this high luminosity is most likely a strong shock interaction with dense local interstellar and/or circumstellar material (CSM). However, the young age of the NGC 4449 SNR may also be an important factor. Similar and even much higher X-ray luminosities have been seen in some historic extragalactic SNe having strong CSM interactions some 10 to 30 years after outburst (e.g., SN 1979C:  $14 \times 10^{38}$  erg s<sup>-1</sup>; SN 1995N:  $175 \times 10^{38}$  erg s<sup>-1</sup>; for 0.1-2.4 keV).

Recent optical spectral line data suggest expansion velocities in the remnant as high as 6000 km s<sup>-1</sup> (Blair & Fesen 1998). Such velocities, when combined with an upper limit for the angular diameter of 0.6 pc from HST observations, imply an age of the SNR is  $\approx 100$  yr. This makes the NGC 4449 SNR only about one tenth as old as G292.0+1.8, N132D, or 1E 0102-7219, and about a third as old as Cas A, the youngest currently known Galactic SNR.

We show in Figure 4 the extracted NGC 4449 SNR spectra compared to the O-rich SNRs Cas A, 1E 0102-7219, and G292.0+1.8. Significant differences can be seen among these four SNR spectra. For example, while G292.0+1.8, 1E 0102-7219, and the NGC 4449 SNR all show emission around the 900 eV Ne IX resonance forest (see Fig. 2), this emission

is nearly absent in Cas A. Also, 1E 0102-7219 is the only SNR shown which exhibits obvious emission at the 574 eV O VII line. Therefore, while there is clearly a range of X-ray spectral properties within the O-rich subclass of SNRs, the X-ray spectrum of the NGC 4449 SNR fits within this range.

Except for G292.0+1.8, there are large differences in the expansion velocity derived from X-rays and that derived from optical emission lines, as shown in Table 2. The shock velocity estimate for the X-ray emitting gas in NGC 4449 SNR is  $830 \text{ km s}^{-1}$ . This is  $\approx 15\%$  higher than that estimated from the spectral fit of Vogler & Pietsch (1997) ( $\approx 700 \text{ km s}^{-1}$ ), but still many times lower than the  $3500 - 6000 \text{ km s}^{-1}$  velocity measured from optical line emission (Blair, Kirshner, & Winkler 1983; Blair & Fesen 1998). Similar differences between X-ray and optical expansion velocities have been seen in other O-rich SNR. Optical studies of Cas A indicate that the ejecta is moving at  $4000 - 6000 \text{ km s}^{-1}$ . However, X-ray analyses suggest that the X-ray emitting gas has a temperature of  $\sim 3.0 \times 10^7 \text{ K}$ , corresponding to a velocity of  $\approx 1900 \text{ km s}^{-1}$ . Similarly, in N132D and 1E 0102-7219 the X-ray shock velocity is only about 20% that of the velocity seen from optical emission studies.

The fact that the X-ray emitting gas exhibits a lower shock velocity than the optically emitting gas is not unexpected. Both optical and X-ray emissions largely arise from SN ejecta interacting with the remnant’s reverse shock that is generated as the SNR forward shock moves through local ISM/CSM material. The reverse shock, traveling back toward the SNR center, will naturally drive a lower velocity shock into the denser optically bright ejecta compared to the lower density, X-ray gas. The higher reverse shock velocity in the X-ray bright gas will lead to greater deceleration of the outward expanding ejecta. Thus, the remnant’s X-ray derived expansion will be corresponding less than that seen in the optical.

An additional factor for explaining the difference between the optically derived expansion velocity and the X-ray gas velocity is that in all cases, equipartition between ion and electron temperatures has been assumed in the X-ray spectral model fits. In general the ions should have a higher temperature, since they carry the bulk of the energy in the shock. If the electrons and ions are not equilibrated, which is possible in collisionless shocks like those found in SNR where equilibrium is reached via Coulomb collisions, then the mean gas temperature should be more heavily weighted toward the ion temperature, implying a X-ray shock velocity closer to the shock velocity seen in optical emissions. Recently, Ghavamian et al. (2002) have found a very low degree of electron-ion equilibration ( $T_e/T_p \leq 0.07$ ) in the SN 1006 remnant. If this sort of non-equilibrium state existed in the NGC 4449 SNR, as well as many of the the other O-rich SNR listed, then that might help to explain the relatively low derived X-ray shock velocities.

### 3.3. SNR Evolution

Kirshner & Blair (1980) suggested that because of its young age and prodigious luminosity, significant changes in the X-ray and optical output of the NGC 4449 SN might be observed on the timescale of just a few years. The 2001 *Chandra* flux reported here may lend support to growing evidence for relatively rapid changes in the remnant’s properties and luminosities.

For example, de Bruyn, Goss, & van Woerden (1981) and de Bruyn (1983) observed a nearly 50% drop in the 6 cm radio flux density between 1973 and 1982. In the optical, whereas 1978 – 1980 spectra taken by Kirshner & Blair (1980) and Blair, Kirshner, & Winkler (1983) found only narrow [S II]  $\lambda\lambda 6716, 6731$  associated with emission from the surrounding H II region, recent spectra obtained in 1995 and 2002 indicate the emergence of broad [S II]  $\lambda\lambda 6716, 6731$  from the SN ejecta (Fesen & Patnaude 2003).

In light of these results, our X-ray flux measurement may likewise indicate changes in the remnant’s X-ray flux over the last 20 years. Both our 2001 *Chandra* and the 1994 *ROSAT* estimated 0.5 – 2.1 keV X-ray luminosity values are only about half of the 1979 *Einstein* 0.2 – 4.0 keV measurements reported by Blair, Kirshner, & Winkler (1983). Although the energy ranges for these flux measurements are different, the observed *Chandra* spectrum does not suggest a significant amount of flux below 0.5 keV or above 2.1 keV. Thus, while there is some uncertainty in the accuracy of comparing *Einstein* and *Chandra* derived fluxes for such a metal-rich SNR, the overall percentage decrease observed is not out of line with reported changes seen in other wavelength regions.

In order to investigate further the reality of these flux changes, we have convolved our NGC 4449 SNR X-ray spectrum model with the telescope response for both the *Einstein* HRI and *ROSAT* HRI. This resulted in a predicted count rate which then could be directly compared to the observed *Einstein* and *ROSAT* count rates for the SNR reported in the literature. The reported *Einstein* and *ROSAT* count rates are most likely overestimated due to source confusion from two nearby X-ray sources (see Fig. 1). To account for this, we assumed that the two nearby sources were stable over the time period 1979 – 2001. We calculated the ratio of the *Chandra* count rates for the two sources to the *Chandra* count rate for the SNR plus the contaminating sources. This percentage was then subtracted from the observed *Einstein* and *ROSAT* count rates to get an adjusted rate. This method assumes that the SNR count rate was also stable between the different observations. Finally, in order to remove telescope dependent effects, we adopted the ratio of the source-adjusted observed rate to the predicted rate.

The ratio of source-adjusted observed to predicted count rate is shown in Figure 5. In



essence, this plot shows the ratio of the observed count rate versus what would be observed by the same telescope in 2001. This figure suggests that the count rate, and thus the remnant’s X-ray luminosity, has dropped nearly 50% over the past 15–20 years. It will be interesting to follow the remnant’s X-ray evolution over the next few decades to see if this trend continues.

#### 4. Conclusions

We have analyzed a 29 ksec *Chandra* ACIS-S observation of the  $\approx 100$  yr old O-rich supernova remnant in the irregular galaxy NGC 4449. We found the following:

1) The spectrum shows the likely presence of several emission lines including O VIII, Ne X, Mg XI, and Si XIII with an overall spectrum similar in appearance to the oxygen-rich Galactic SNR G292.0+1.8.

2) We find an X-ray luminosity of  $2.4 \times 10^{38}$  erg  $s^{-1}$ , for the energy range 0.5 – 2.1 keV and a distance of 3.9 Mpc. Assuming a spherical geometry for the remnant we estimate the mass of the X-ray emitting gas, including the mass of metals as well as He and H, to be  $M_{\text{Xray}} \approx 5.7 f D_{3.9\text{Mpc}}^{2.5} M_{\odot}$ .

3) A non-equilibrium ionization fit to the spectrum suggests a large overabundance of oxygen of  $\approx 18$  times solar, consistent with the remnant’s UV and optical emission-line properties.

4) Based on electron-ion temperature equilibration, we derive an X-ray shock velocity of  $\approx 830$  km  $s^{-1}$ . This is significantly lower than the 6000 km  $s^{-1}$  optical expansion velocity determined from optical measurements but consistent with differences between the optical and X-ray velocities seen in other O-rich remnants.

5) While our estimated X-ray flux is in rough agreement with that measured by *ROSAT* in 1994, it is only about half of that of an 1978 *Einstein* observation. Despite uncertainties in the accuracy of such flux measurement comparisons, such a decrease would not be unexpected given recent measurements made in the radio and optical suggesting that the remnant continues to undergo significant changes since its discovery in 1978.

The NGC 4449 SNR’s current standing as the youngest and most luminous O-rich remnant known certainly make it an object worthy of continued study. The remnant’s estimated angular dimensions of  $\approx 0''.028$  make it an ideal candidate for VLBI measurements of its true size and emission sub-structure, like that accomplished for SN 1993J (Bietenholz, Bartel, & Rupen 2001). Such measurements could help clarify its general structure and, when combined with optical emission line width data, set strict limits on its expansion age.

The authors wish to thank Robert Petre and Randall Smith for useful comments during the preparation of this manuscript, Dick Edgar for help with fitting the data, and John Raymond for helpful discussions regarding the effects of non-equipartition in the plasma temperature. We also thank the anonymous referee for useful suggestions and a careful reading of this manuscript.

## REFERENCES

- Balick, B. & Heckman, T. 1978, *ApJ*, 226, L7
- Bautz, M. W. et al. 1998, *Proc. SPIE*, 3444, 210
- Bietenholz, M. F., Bartel, N., & Rupen, M. P. 2001, *ApJ*, 557, 770
- Blair, W. P. & Fesen, R. A. 1998, *BAAS*, 193, 7404
- Blair, W. P., Kirshner, R. P., & Winkler, P. F. 1983, *ApJ*, 272, 84
- Blair, W. P., Raymond, J. C., Fesen, R. A., & Gull, T. R. 1984, *ApJ*, 279, 708
- Churazov, E., Gilfanov, M., Forman, W., & Jones, C. 1996, *ApJ*, 471, 673
- de Bruyn, A. G., Goss, W. M., & van Woerden, H. 1981, *A&A*, 94, L25
- de Bruyn, A. G. 1983, *A&A*, 119, 301
- de Vaucouleurs, G., de Vaucouleurs, A., Corwin, H. G., Buta, R. J., Paturel, G., & Fouque, P. 1991, *Third Reference Catalogue of Bright Galaxies* (New York: Springer)
- Fesen, R. A., & Patnaude, D. J. 2003, in preparation
- Garmire, G. P. et al. 1992, *American Institute of Aeronautics and Astronautics Conference*, 24
- Ghavamian, P., Winkler, P. F., Raymond, J. C., & Long, K. S. 2002, *ApJ*, 572, 888
- Hughes, J. P. 1987, *ApJ*, 314, 103
- Hughes, J. P. & Singh, K. P. 1994, *ApJ*, 422, 126
- Hunter, D. A., van Woerden, H., & Gallagher, J. S. 1999, *AJ*, 118, 2184
- Jerius, D., Donnelly, R. H., Tibbetts, M. S., Edgar, R. J., Gaetz, T. J., Schwartz, D. A., Van Speybroeck, L. P., & Zhao, P. 2000, *Proc. SPIE*, 4012, 17

- Kirshner, R. P. & Blair, W. P. 1980, *ApJ*, 236, 135
- Peimbert, M. 1971, *ApJ*, 170, 261
- Sabbadin, F. & Bianchini, A. 1979, *PASP*, 91, 28
- Seaquist, E. R. & Bignell, R. C. 1978, *ApJ*, 226, L5
- Seward, F., Slane, P., Smith, R., Gaetz, T., Coe, B. C., & Lee, B. B. 2002, “Chandra Supernova Remnants Catalog”, <http://hea-www.harvard.edu/ChandraSNR>
- van den Bergh, S. 1988, *ApJ*, 327, 156
- Vogler, A. & Pietsch, W. 1997, *A&A*, 319, 459
- Weisskopf, M. C., O’Dell, S. L., & van Speybroeck, L. P. 1996, *Proc. SPIE*, 2805, 2

Table 1. Best-Fit Parameters for NEI Model

Parameter	NGC 4449 <sup>a</sup>	G292.0+1.8 <sup>a,b</sup>
$N_H$ (atoms $\text{cm}^{-2}$ )	$(1.7 \pm 0.06) \times 10^{21}$	$(8.0_{-1.98}^{+0.68}) \times 10^{21}$
kT (keV)	$0.80_{-0.20}^{+0.28}$	$1.64_{-0.19}^{+0.29}$
$n_e t$ (s $\text{cm}^{-3}$ )	$(1.18 \pm 0.04) \times 10^{12}$	$(5.55_{-1.1}^{+1.2}) \times 10^{10}$
$\langle kT \rangle$ (keV)	$1.19_{-0.07}^{+0.09}$	...
$n_H n_e V$ ( $\text{cm}^{-3}$ ) <sup>c</sup>	$(0.55 \pm 0.05) \times 10^{61}$	$(0.43 \pm 0.37) \times 10^{58}$
$n_O n_e V / [\text{O}/\text{H}]_{\odot}$ ( $\text{cm}^{-3}$ )	$(10.0_{-3.8}^{+6.7}) \times 10^{61}$	$(22.6_{-3.2}^{+2.7}) \times 10^{58}$
$n_{\text{Ne}} n_e V / [\text{Ne}/\text{H}]_{\odot}$ ( $\text{cm}^{-3}$ )	$(2.0_{-1.4}^{+1.5}) \times 10^{61}$	$(6.4_{-3.2}^{+2.7}) \times 10^{58}$
$n_{\text{Mg}} n_e V / [\text{Mg}/\text{H}]_{\odot}$ ( $\text{cm}^{-3}$ )	$(4.8_{-2.7}^{+2.8}) \times 10^{61}$	$(7.88 \pm 0.40) \times 10^{58}$
$n_{\text{Si}} n_e V / [\text{Si}/\text{H}]_{\odot}$ ( $\text{cm}^{-3}$ )	$(5.1_{-1.6}^{+1.7}) \times 10^{61}$	$(2.14 \pm 0.14) \times 10^{58}$
$n_{\text{Fe}} n_e V / [\text{Fe}/\text{H}]_{\odot}$ ( $\text{cm}^{-3}$ )	$(1.2_{-0.3}^{+0.3}) \times 10^{61}$	$(3.0_{-1.0}^{+1.1}) \times 10^{58}$
$[\text{O}/\text{H}] / [\text{O}/\text{H}]_{\odot}$	$18.0_{-6.5}^{+12.0}$	...
$[\text{Ne}/\text{H}] / [\text{Ne}/\text{H}]_{\odot}$	$15.0_{-10.0}^{+12.0}$	...
$[\text{Mg}/\text{H}] / [\text{Mg}/\text{H}]_{\odot}$	$9.0_{-5.0}^{+5.5}$	...
$[\text{Si}/\text{H}] / [\text{Si}/\text{H}]_{\odot}$	$9.0_{-3.0}^{+3.1}$	...
$[\text{Fe}/\text{H}] / [\text{Fe}/\text{H}]_{\odot}$	$2.2_{-0.5}^{+0.6}$	...
$\chi^2$ (d.o.f)	292 (266)	154 (130)

<sup>a</sup>Statistical errors at 90% confidence.

<sup>b</sup>Values quoted from Hughes & Singh 1994.

<sup>c</sup>Emission measure scaled by solar abundance relative to H. Assumes a distance of 3.9 Mpc to NGC 4449, and SNR radius of 0.3 pc. For the best fit values of the parameters in the table,  $n_e/n_H = 1.47$ .

Table 2. Comparison of O-rich SNR

Object	Distance (kpc)	$F_X^a$ ( $10^{-14}$ erg $\text{cm}^{-2}$ $\text{s}^{-1}$ )	$L_X$ ( $10^{38}$ erg $\text{s}^{-1}$ )	Age (yr)	$V_{\text{opt}}$ ( $\text{km s}^{-1}$ )	$V_{X\text{-ray}}$ ( $\text{km s}^{-1}$ )	References
NGC 4449 SNR <sup>b</sup>	3900	8.6	2.4	$\sim 100$	6000	830	1,2,3,4
G292.0+1.8 <sup>c</sup>	4.8	$2.0 \times 10^5$	0.06	$< 1600$	1100	1200	5,6,7
Cas A <sup>c</sup>	3.4	$1.9 \times 10^6$	.26	320	6000	1900	6,7
N132D <sup>c</sup>	49	$3.3 \times 10^4$	0.9	$\sim 1350$	3400	790	6,7
1E 0102.1-7219 <sup>c</sup>	72	$5.8 \times 10^3$	$3.4 \times 10^{-3}$	$\sim 1000$	4000	610	6,7

<sup>a</sup>Unabsorbed flux determined from fitting a two component thermal plasma with variable abundances.

<sup>b</sup>For the energy range 0.5 – 2.1 keV.

<sup>c</sup>For the energy range 0.3 – 2.0 keV.

References. — (1) Balick & Heckman 1978; (2) Seaquist & Bignell 1978; (3) Blair, Kirshner, & Winkler 1983; (4) Blair & Fesen 1998; (5) Hughes & Singh 1994; (6) Seward et al. 2002; (7) van den Bergh 1988

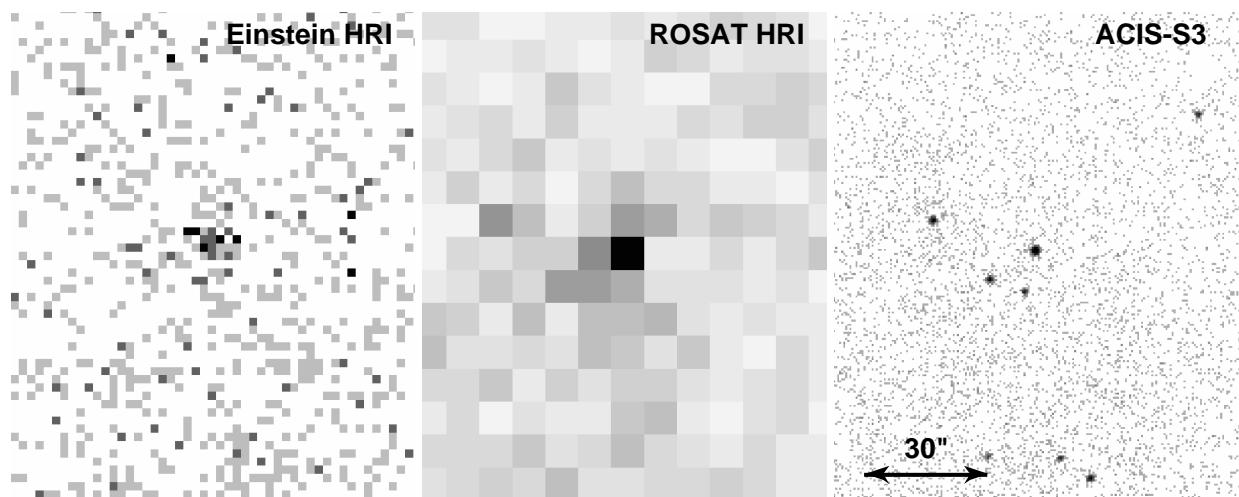


Fig. 1.— Einstein HRI, ROSAT HRI, and Chandra ACIS-S images of the SNR in NGC 4449.

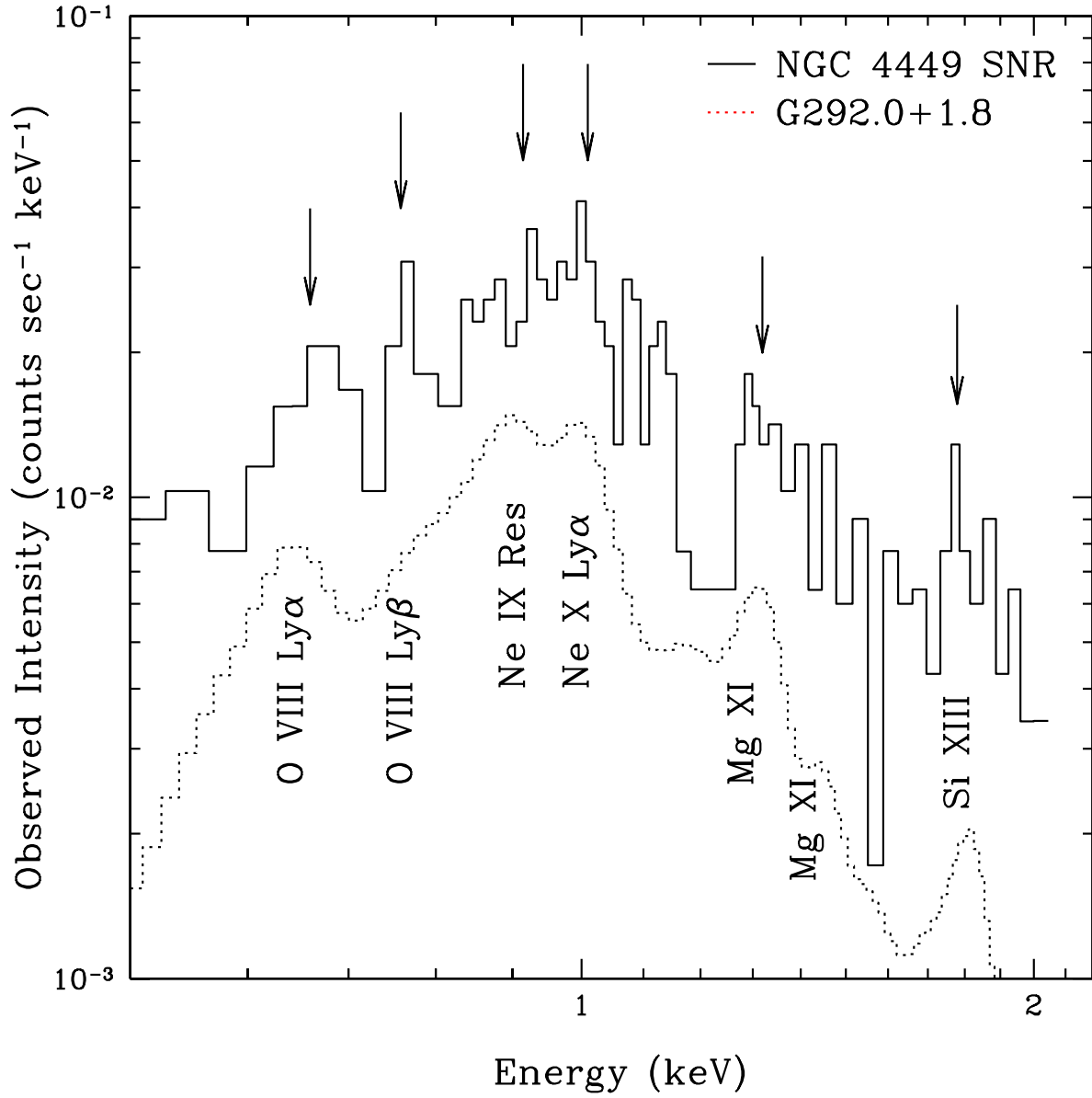


Fig. 2.— Comparison between the SNR in NGC 4449 and SNR G292.0+1.8. The observed intensity of G292.0+1.8 has been arbitrarily scaled down by a factor of 8000 so that a comparison of detected lines between the two SNRs may be made. No correction for Galactic extinction has been included.

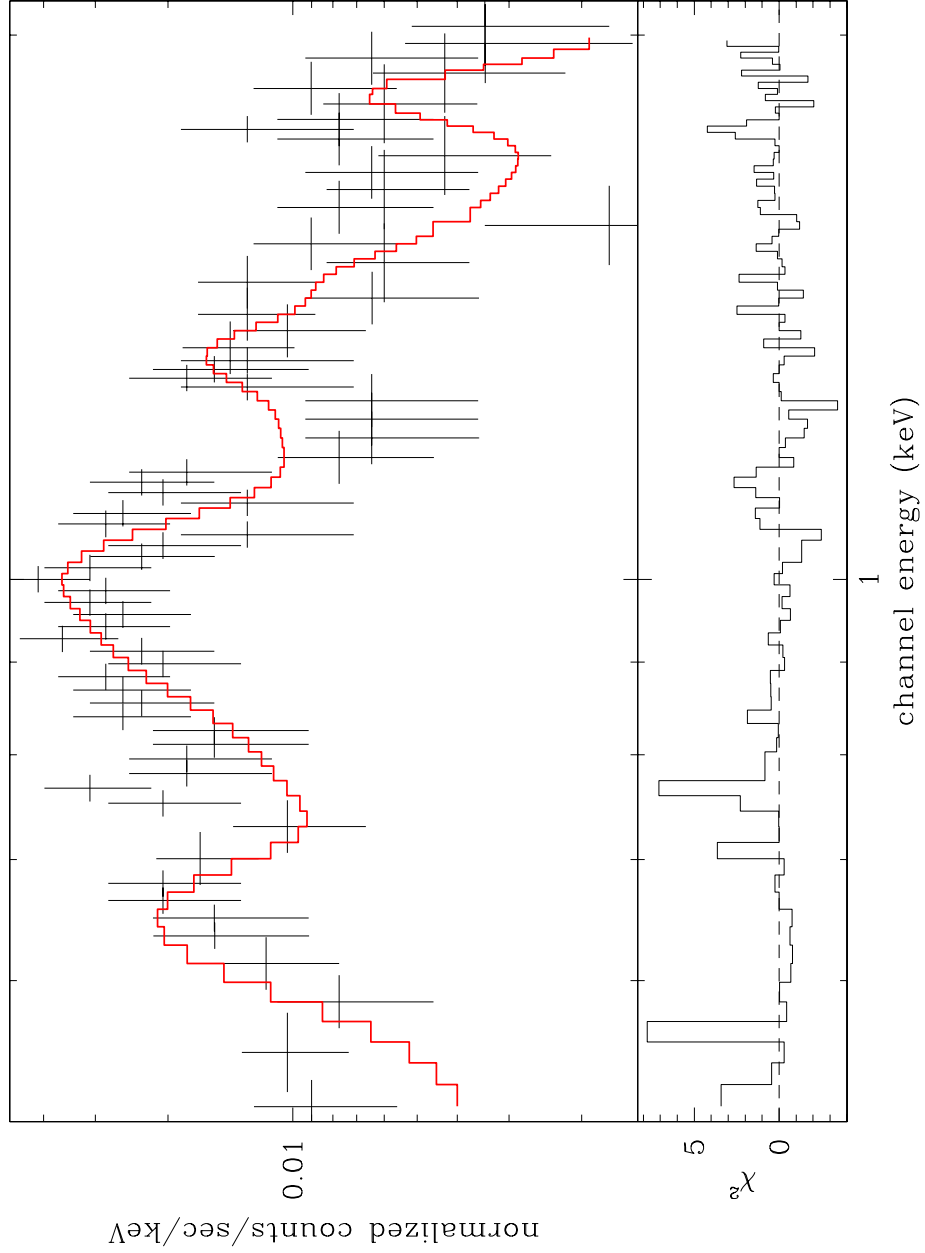


Fig. 3.— Model fit to the spectrum extracted from the NGC 4449 SNR.

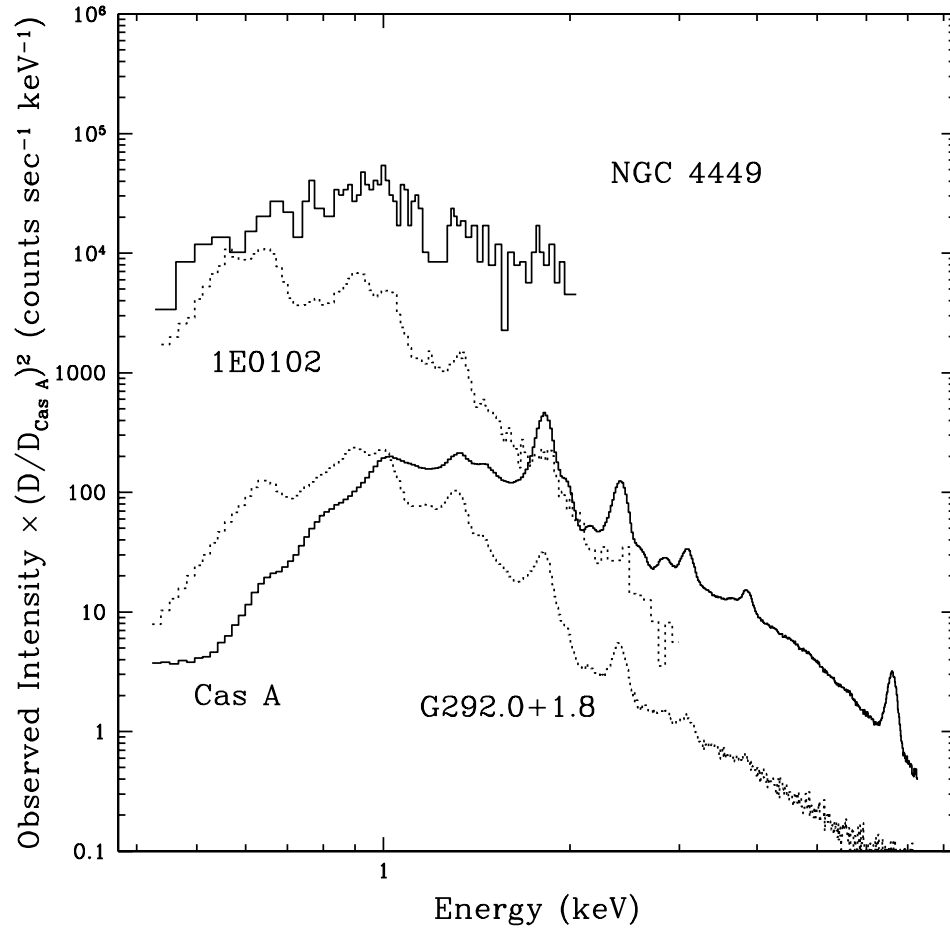


Fig. 4.— Spectra for four oxygen-rich SNR. Each spectrum is for the whole remnant, scaled to a distance of 3.4 kpc. No corrections for Galactic extinction have been made.



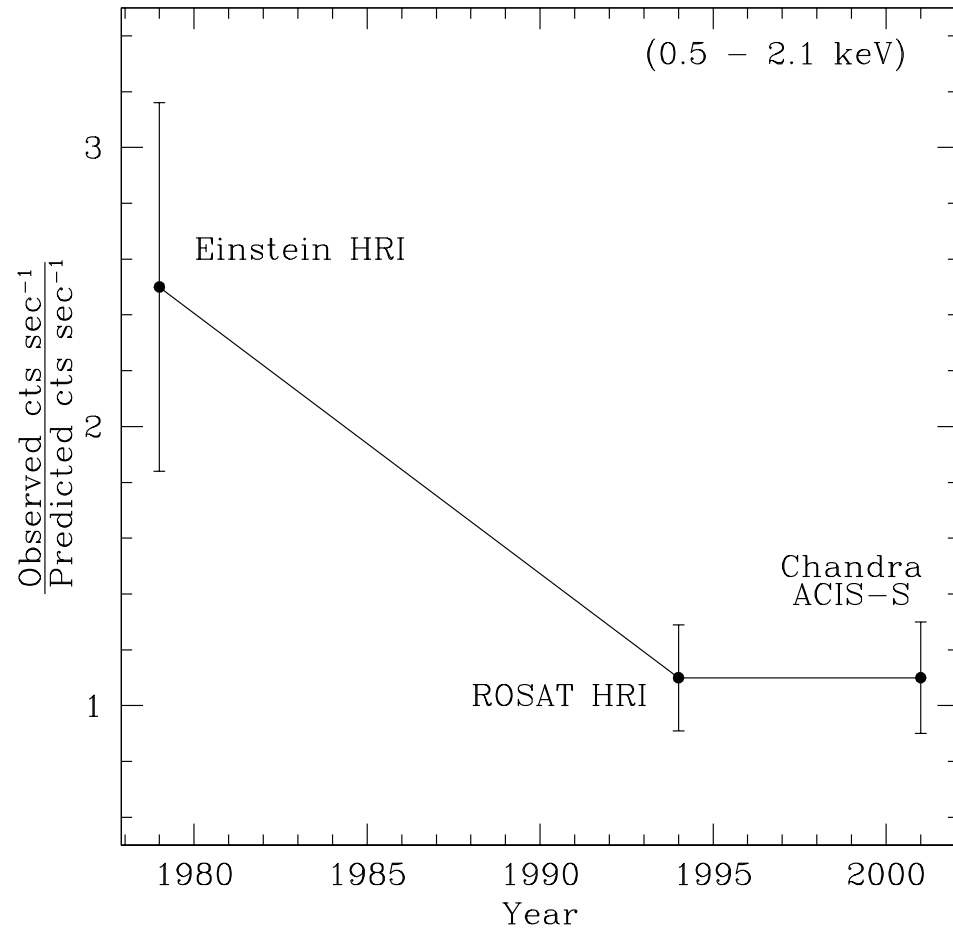


Fig. 5.— Ratio of the observed count rates over three observations versus count rates predicted by convolving our NEI model with the telescope responses.